Functional Oxide Nanomaterials and Nanocomposites for the Removal of Heavy Metals and Dyes

Invited Review Article

Sarika Singh[1], K. C. Barick[2] and D. Bahadur[1,*]

1 Department of Metallurgical Engineering and Materials Science, Indian Institute of Technology Bombay, Mumbai
2 Chemistry Division, Bhabha Atomic Research centre, Mumbai
* Corresponding author E-mail: dhirenb@iitb.ac.in

Abstract Water scarcity and its contamination with toxic metal ions and organic dyes represent a serious worldwide problem in the 21st century. A wide range of conventional approaches have been used to remove these contaminants from waste. Recently, nanotechnology has been given great scope for the fabrication of desirable nanomaterials with large surface-to-volume ratios and unique surface functionalities to treat these pollutants. Amongst these, oxide-based nanomaterials emerge as promising new materials for water purification. In this review article, we explore a broad-spectrum overview of recent developments in the area of oxide-based nanomaterials, such as Fe_3O_4, ZnO and TiO_2, as well as their binary and ternary nanocomposites, for the removal of various toxic metal ions and organic dyes. The possible adsorption mechanism and the surface modification of adsorbents for the removal of heavy metal ions and dyes are discussed in detail. The sorption properties of the different adsorbents depend on the surface functionalization of nanomaterials, the pH of the medium, and the reaction time and concentration, etc. In addition, we provide a short overview on the study of the selective adsorbents in multi-component sorption systems, along with the future prospects of oxide nanomaterials in water purification.

Keywords Nanomaterials, Oxides, Nanocomposite, Water-Purification, Toxic Metal Ions, Photocatalysis

1. Introduction

Today's world faces alarming challenges in the rising demand for clean drinking water, and conditions are particularly bad in developing countries [1]. The scarcity of water in terms of both quantity and quality has become a significant threat to the well-being of humanity. In particular, the quality of drinking water has become a serious concern, with the rapid escalation of industrialization towards a developed society. The waste products generated from the textiles, chemicals, mining and metallurgical industries are mainly responsible for contaminating the water [2,3]. This contaminated water contains non-biodegradable effluents, such as heavy metal ions (arsenic, zinc, copper, nickel, mercury, cadmium, lead and chromium, etc.) and organic materials

that are carcinogenic to human beings and harmful to the environment [4,5].

Water contaminated with arsenic (As) has been a serious issue, especially in Vietnam, Bangladesh and some other countries. Long-term exposure to arsenic via drinking-water causes cancer of the skin, the lungs, the urinary bladder and the kidney, as well as other skin problems such as pigmentation changes and thickening (hyperkeratosis). As per some estimations, arsenic in drinking water will cause 200,000-270,000 deaths from cancer in Bangladesh alone [6]. Another toxic metal pollutant is lead which, if present with a concentration of >70 µg/dL in blood levels (WHO), can damage various bodily systems, including the nervous and reproductive systems and the kidneys, and it can also cause high blood pressure and anaemia. Large amounts of lead (>100 µg/dL) in the body can lead to convulsions, coma and death [7]. According to the WHO, the limit of the toxicity value for nickel is 130 µgL^{-1}, assuming a 60 kg adult drinking two litres of water per day. However, the presence of nickel at higher levels in the human body can cause serious lung and kidney problems as well as gastrointestinal distress, pulmonary fibrosis and skin dermatitis [8]. A further neurotoxin is mercury, which can cause damage to the central nervous system, and its concentration within the range of 0.12–4.83 mgL^{-1} may cause the impairment of pulmonary and kidney function, chest pain and dyspnoea [9]. As per the U.S. Environmental Protection Agency, cadmium is a plausible human carcinogen, and its presence potentially damages human physiology and other biological systems when the tolerance levels are exceeded. High levels of cadmium exposure (1 mgm^{-3}) may result in several complications leading to death [10].

In addition to heavy metal contaminants, other hazardous contaminants found in the environment are organic dyes, discharged from textile manufacture and other industrial processes into the water. The dyes presently used in industries include methylene blue (MB), Rhodamine B (RhB), methyl orange (MO), Rhodamine 6G (Rh6G) as well as organic chemicals (phenol and toluene), and the release of these into lakes or other water sources has become a serious health concern [11]. Various treatment techniques and processes have been developed for the removal of toxic contaminants from wastewater, such as adsorption, ion exchange, chemical precipitation, membrane-based filtration, photodegradation, evaporation, solvent extraction, reverse osmosis, and so on [12-18]. Among these, adsorption and photodegradation are conventional but efficient techniques for removing toxic contaminants from water [19,20]. For this, numerous adsorbents/catalysts have been developed for the removal of such hazardous chemicals from wastewater. However, most of them suffer from certain drawbacks, such as high capital and operational costs for treatment, and the disposal of the residual metal sludge [21]. Thus, there is urgent demand for the development of low-cost materials and better processes for providing clean drinking water (i.e., free from contaminants such as toxic chemicals and metal ions).

Nanotechnology is considered as having the potential to play an important role in shaping our current environment by providing new materials, remediation/treatment techniques and sensors for monitoring purposes [22]. For water purification, there is a need for technologies that have the ability to remove toxic contaminants from the environment to a safe level and to do so rapidly, efficiently and within a reasonable costs framework. Thus, the development of novel nanomaterials with increased affinity, capacity and selectivity for heavy metals and other contaminants is an active emerging area of research in the field of nanotechnology. The benefits of using nanomaterials are mainly associated with their large specific surface area and high reactivity. These nanomaterials can be used to improve water quality and the availability and viability of water resources, such as through advanced filtration, which enables sustainable water reuse, recycling or desalination.

A variety of efficient, cost-effective and environmentally-friendly nanomaterials have been developed, each possessing unique functionality in their potential application to the detoxification of industrial effluents, groundwater, surface water and drinking water. Among the various kinds of nano-adsorbents, oxide-based nanomaterials such as Fe_3O_4, TiO_2, ZnO and their composites play an important role. These nanomaterials have various applications in many scientific and industrial fields, including wastewater purification, catalysis and magnetic devices [22-25]. Recently, there have been several reports on magnetic oxides, especially Fe_3O_4, being used as nano-adsorbents for the removal of various toxic metal ions from wastewater, such as Ni^{2+}, Cr^{3+}, Cu^{2+}, Cd^{2+}, Co^{2+}, Hg^{2+}, Pb^{2+} and As^{3+} [26-31]. These Fe_3O_4 nano-adsorbents are effective and economical for the rapid removal and recovery of metal ions from wastewater effluents due to their large surface area and optimal magnetic properties. They can be reused after magnetic separation in removing the adsorbed toxic contaminants [26,31,32]. Moreover, their surface modification by the attachment of inorganic shells and organic molecules stabilizes and prevents the oxidation of nanoparticles. In addition, these surface functionalities provide sites for the uptake of specific/selective metal ions and, thus, enhance the efficiency of their removal.

Further, some semiconductor metal oxides, including ZnO and TiO_2, have also received a great deal of attention

in the successful photocatalytic degradation of organic contaminants and the adsorption of heavy metals [33-37]. In particular, these materials have attracted much attention because of theirs high photosensitivity, higher absorption capacity, better quantum efficiency, non-toxicity and wide band-gap. These nanoparticles with a high surface area and porosity exhibit higher photocatalytic activity than their bulk counterparts by minimizing the distance between the sites of photon absorption and preventing the electron–hole (e^--h^+) recombination. Also, numerous oxide-based nanocomposite/hybrid materials have been developed for water purification. These are composed of two or more components, and thus can exhibit the properties of multicomponent systems in the same material [38-41]. There are considerable challenges remaining in environmental remediation, especially in terms of large-scale applications.

Due to the alarming challenges in the rising demand for clean drinking water, researchers from both academia and industry have been keenly involved in the development of new materials and methods for the purification of water. The importance of research in this area can be well understood from the availability of a large number of review articles on water purification in the literature. Many of them are dedicated to various techniques for the removal of heavy metal ions and organic contaminants, as well as their various advantages and limitations [19,42]. The present review mainly deals with the development of low-cost, efficient and reusable novel oxide-based nanomaterials for providing clean drinking water. The importance of the surface engineering/modification of nanomaterials with various functional groups for the capture of toxic metal ions is discussed in this review. We have also included various oxide-based binary and ternary nanocomposites that have been developed for the removal of pollutants from water.

2. Oxide nanomaterials in water purification

2.1 Removal of heavy metal ions

2.1.1 Fe₃O₄ nanoparticles

Magnetic nanoparticles are gaining in importance, as they can be used as highly effective, efficient and economically-viable adsorbents, with the additional advantage of their easy separation under a magnetic field for reuse. Many of these reports deal with the influence of different parameters on the removal of metal ions by Fe_3O_4 magnetic nanoparticles [43-46]. Shen et al. [43], for example , have observed that the adsorption efficiency of Ni^{2+}, Cu^{2+}, Cd^{2+} and Cr^{6+} ions by Fe_3O_4 nanoparticles is strongly dependent on pH, temperature, the amount of

the adsorbent and the incubation time. Further, they have found a higher removal efficiency of these metal ions at a 3.5 mg mL^{-1} dose of nano-adsorbent with an optimum pH of four.

In comparison to bare Fe_3O_4 nanoparticles, surface-functionalized Fe_3O_4 nanoparticles have been extensively used for the removal of toxic metal ions [26-31,47-51]. Singh et al. [31] reported the removal of toxic metal ions from wastewater by using carboxyl-, amine- and thiol-functionalized Fe_3O_4 nanoparticles (succinic acid, ethylenediamine and 2,3-dimercaptosuccinic acid, respectively). Depending upon the surface functionality ($COOH$, NH_2 or SH), these magnetic nano-adsorbents capture metal ions either by forming chelate complexes, by ion exchange process or else through electrostatic interaction. It has been observed that these surface-engineered Fe_3O_4 nanoparticles have a strong affinity for the simultaneous adsorption of Cr^{3+}, Co^{2+}, Ni^{2+}, Cu^{2+}, Cd^{2+}, Pb^{2+} and As^{3+} from wastewater (Figure 1A). In addition, the adsorption process was found to be highly dependent on the amount, surface functionality and pH of the medium, which caused these nanoparticles to selectively adsorb metal ions. An almost 100% removal rate of Cr^{3+}, Co^{2+}, Ni^{2+}, Cu^{2+}, Cd^{2+} and Pb^{2+} ions from water was observed at pH > 8 by these functionalized nanoparticles. The removal efficiency of As^{3+} by carboxyl, amine and thiol-functionalized Fe_3O_4 was found to be 91%, 95% and 97%, respectively, at pH 8. The adsorption-desorption behaviour of metal ions on amine-functionalized Fe_3O_4 showed an 85% desorption ratio in the first cycle (Figure 1B), which indicates their excellent regeneration capacity for their further use. They also prepared ethylenediamine tetraacetic acid-functionalized (EDTA) Fe_3O_4 nanomagnetic chelators (NMCs), which show a strong tendency towards the adsorption of Cr^{3+}, Co^{2+}, Ni^{2+}, Cu^{2+}, Cd^{2+} and Pb^{2+} from wastewater [47]. Ozmen et al. [48] have reported the use of 3-aminopropyltriethoxysilane and glutaraldehyde-modified Fe_3O_4 nanoparticles for the removal of Cu^{2+} from water. Ge et al. [49] have studied the effective removal of heavy metal ions (Cd^{2+}, Zn^{2+}, Pb^{2+} and Cu^{2+}) from an aqueous solution using polymer-modified magnetic nanoparticles. They reported a higher removal efficiency of metal ions in acidic pH 5.5 and a lower one in alkaline pH. Based on their results, they have suggested that the polymer-modified Fe_3O_4 was more efficient than bare Fe_3O_4. All of the above studies clearly suggest that the functional groups present on the surface of magnetic nanoparticles provide a large number of active sites as well as aqueous stability, which is necessary for the successful adsorption of toxic metal from water. More specifically, these surface-engineered magnetic nanoparticles are highly effective, efficient and economically viable and reusable magnetic nano-adsorbents for the removal of toxic metal ions from water.

www.intechopen.com

Sarika Singh, K. C. Barick and D. Bahadur: Functional Oxide Nanomaterials and Nanocomposites for the Removal of Heavy Metals and Dyes   3

Magnetic nanoparticles were also successfully used for the separation of toxic metal ions from different sources. Wang et al. [50] have reported rhodamine hydrazide-modifying Fe_3O_4 microspheres (Fe_3O_4-R6G) for the selective detection and removal of mercury ions from different environmental samples, such as tap water, lake water (Linghu Lake, Anqing, China) and river water (Changjiang River, Anqing, China). They found that 1.5×10^{-7} mol L^{-1} is the detection limit for Hg^{2+} and that 37.4 µmolg^{-1} is the maximum adsorption of Hg^{2+} in a 3 mL sample with 5 mg Fe_3O_4-R6G. The adsorption of Hg^{2+} onto Fe_3O_4-R6G was confirmed with the shift in binding energy from X-ray photoelectron spectroscopy (XPS) analysis. They also studied the regeneration capability for up to three cycles, and observed that it could reversibly bind with Hg ions repeatedly. Warner et al. [51] have used surface-functionalized Fe_3O_4 nanoparticles for the separation of heavy metals in Columbia River water. They introduced a large number of surface-functional groups onto the surface of magnetic nanoparticles by functionalizing them with EDTA, l-glutathione, mercaptobutyric acid, thiolated-PEG and meso-2,3-dimercaptosuccinic acid, for the enhancement of the adsorption capacity of toxic metals. They have observed that the magnetic nanoparticles functionalized with the thiol and EDTA moiety exhibit a strong binding potential towards specific heavy metal ions. They compared the removal efficiency of these surface-functionalized Fe_3O_4 nanoparticles with selected commercial sorbents with similar surface functionality, as well as bare iron oxide nanoparticles, and found that surface-functionalized particles have a higher tendency for the removal of toxic metal ions. In brief, their adsorption efficiency is dependent on their surface functionality, the competitive affinity of metal ions, the amount of surface charge and the availability of active surface sites on nanoparticles.

2.1.2 ZnO nanoparticles

Zinc oxide is a promising candidate for the removal of contaminants and environmental remediation. It has many surface active sites for the adsorption of heavy metal ions from an aqueous solution. Further, ZnO nanoparticles with a porous micro/nanostructure provide an ample surface area for the adsorption of heavy metal ions from contaminated water. Recently, there have been reports on the adsorption of heavy metal ions using porous micro/nanostructured materials with different morphologies, such as nano-assemblies, nano-plates, hierarchical ZnO nano-rods and microspheres with nano-sheets as absorbents [34,36,52-54]. Wang et al. [34,52] demonstrated the higher efficiency of porous ZnO nano-plates and ZnO hollow microspheres with exposed porous nano-sheets in the removal of Cu(II) from contaminated water when compared with commercial ZnO (Figure 1C). These nano-plates and microspheres showed an unsaturated adsorption capacity for Cu(II) ions, whereas that of commercial ZnO nano-powders is saturated at around 300 mg g^{-1}. They have attributed this enhanced adsorption of heavy metal ions to their unique micro/nanostructure. Singh et al. [36] reported on the removal of various toxic metal ions, such as Co^{2+}, Ni^{2+}, Cu^{2+}, Cd^{2+}, Pb^{2+}, Hg^{2+} and As^{3+} from wastewater by porous ZnO nano-assemblies. It was reported that Hg^{2+}, Pb^{2+} and As^{3+} have a stronger attraction towards ZnO nano-assemblies due to their high electronegativity and, hence, that they exhibit better removal efficiency (63.5% Hg^{2+}, 100% Pb^{2+} and 100% As^{3+}). Kumar et al. [53] have demonstrated the removal of Pb(II) and Cd(II) under different adsorbate concentrations, contact times, adsorbent dosages, pHs and temperature conditions, from aqueous solutions by mesoporous hierarchical ZnO nano-rods. They observed the maximum adsorption capacities of Pb(II) and Cd(II) to be 160.7 and 147.25 mg g^{-1}, respectively, and that the loading capacities of recycled ZnO nano-rods have two-thirds that of their original capacities. Similarly, Sheela et al. [54] used ZnO nanoparticles of size 25 nm for the removal of Cd(II) and Hg(II) ions from an aqueous solution. They found a maximum adsorption capacity of 387 and 714 mg g^{-1} for Cd(II) and Hg(II) ions, respectively. In addition, Ma et al. [55] reported on a novel strategy to prepare ZnO/PbS heterostructured functional nanocomposites based on Pb^{2+} sorbed ZnO. They prepared ZnO nano-sheets via a hydrothermal approach, which exhibited a good sorption capacity for Pb^{2+} (6.7 mg g^{-1}) due to the presence of surface hydroxyl groups.

2.1.3 TiO₂ nanoparticles

Titanium dioxide is another semiconducting material that has been widely used as a powerful adsorbent for the removal of Cr(VI) [37], Cd(II) and Cu(II) [56], As (III) [57,58] and multiple metals (Pb, Cd, Cu, Zn and Ni) [59]. Parida et al. [37] have examined the removal of Cr (VI) by TiO_2-immobilized mesoporous MCM-41. They found 91% absorption of Cr(VI) from a solution containing 100 mgL^{-1} Cr(VI) metal ions in 80 min at pH ~ 5.5 and 323 K. Visa et al. [56] developed a substrate by hydrothermal processing from fly ash coated with TiO_2 and investigated their influence on the adsorption capacity of heavy metal ions (Cu^{2+} and Cd^{2+}) from synthetic wastewater. They observed that the removal efficiency of the fly ash–TiO_2 substrate is much higher for Cu^{2+} from the solution. Jing at al. [57] evaluated the simultaneous removal of As(V), As(III), monomethylarsonic acid (MMA) and dimethylarsinic acid (DMA) in contaminated ground water. Luo at al. [58] have also demonstrated the high absorption capacity, recovery and reuse of TiO_2

nanoparticles for the removal of As(III) from copper smelting wastewater (Figure 1D). They found a reduction of 59 ± 79 μg L^{-1} of As(III) at pH 7 after 21 successive treatment cycles using regenerated TiO$_2$ containing 3890 ± 142 mg L^{-1} As(III) in the wastewater. Engates et al. [59] have studied absorption of single and multi-metal ions by TiO$_2$ nanoparticles and compared the results with those obtained by bulk particles. They have found a 100% removal efficiency of Pb, Cd and Ni ions at 0.1 g L^{-1} within 120 min, which is five-times greater than the bulk particles at the same concentration. They also observed the good photostability of TiO$_2$ nanoparticles after eight cycles at pH 8, whereas the bulk particles were exhausted after three cycles. A similar study conducted by Liang et al. [60] reported on the adsorption capacity of Zn and Cd by nano-TiO$_2$ of size 10–50 nm were 15.3 and 7.9 mgg^{-1}, respectively, at pH = 9. Further, they observed that the presence of common cations and anions (100–5000 mgL^{-1}) has no significant influence on the adsorption of Zn^{2+} and Cd^{2+} ions.

It is worth mentioning here that Fe$_3$O$_4$ magnetic nanoparticles are a widely used and economically viable and reusable nanoadsorbent for the effective removal of toxic metal ions from water as compared to the nano-particulates of non-magnetic oxides. Furthermore, a large and varied literature is available on the removal of toxic metal ions by Fe$_3$O$_4$-based nanocomposites, and some of this research is discussed in the next subsection.
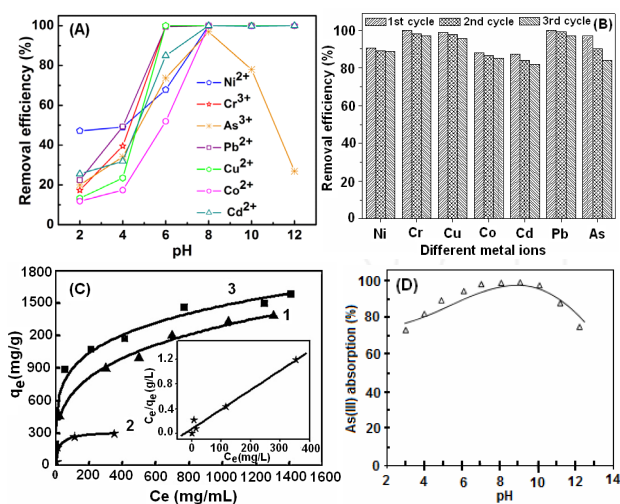

Figure 1. (A) Removal of toxic metal ions by thiol-functionalized (DMSA) Fe$_3$O$_4$ nanoparticles at different pHs [31]; (B) recycling capability of ethylenediamine-functionalized Fe$_3$O$_4$ up to the 3rd generation [31]; (C) removal of Cu(II) ions on porous ZnO nano-sheets with hollow microspheres (curve 1), commercial ZnO powders (curve 2) and porous ZnO nano-plates (curve 3). The inset of Figure 1A shows the plot of $C_e/q_e \sim C_e$ corresponding to curve 2 [34] and (D) the removal of As (III) at different pHs using TiO$_2$ nanoparticles [58] (Reproduced with permission from [31,34] copyright Elsevier and [58] copyright American Chemical Society publications).

2.1.4 Fe$_3$O$_4$-based nanocomposites

Numerous nanocomposites/hybrid materials have been explored for environmental remediation as they exhibit the properties of different components in the same structure. There are reports on the use of core-shell silica magnetic nanoparticles for the removal of metal ions [38,61-64]. Silica shells with different functional groups can efficiently prevent the aggregation and chemical decomposition of Fe$_3$O$_4$ in addition to their strong affinity for capturing of metal ions.

Zhang et al. [38] recently reported on the use of monodisperse amine-terminated Fe$_3$O$_4$@SiO$_2$–NH$_2$ for the removal of metal ions. These amine-terminated core-shell magnetic nanoparticles saw the effective removal of Pb^{2+} within the pH range of 2-6, with an easy recovery capacity via an external magnet. The percentage adsorption of Pb(II) increases with the amino group content in the amine-terminated core-shell nanostructure, revealing that the amino groups worked as efficient chelating sites for Pb(II) adsorption under specific conditions. Their adsorption isotherm and kinetics were well fitted to the Langmuir model and the pseudo-second-order rate equation.

Zhang et al. [61] have studied in detail the formation of Fe$_3$O$_4$–SiO$_2$-poly(1,2-diaminobenzene) core-shell (FSPs) particles of sub-micron size with saturated magnetization of 60–70 emu/g, and utilized them for the removal of As(III), Cu(II) and Cr(III) ions from an aqueous solution (Figure 2A). They investigated the adsorption isotherms of heavy metals with two different wastewater samples: (a) metallurgical refinery wastewater (Zhuzhou, China) and (b) river water (Beidou River, Ningbo, China). They found that the adsorption isotherm data of As(III), Cu(II), and Cr(III) fitted well with the Freundlich model. Further, adsorption efficiency was found to be a strong function of the initial pH value, the amount of the dosage of FSPs and individual metal concentrations.

Recently, Yuan et al. [62] prepared Fe$_3$O$_4$@SiO$_2$@meso-SiO$_2$ microspheres with a large pore size and a greater number of multifunctional amine groups for the adsorption of heavy metal ions. They observed that most of the metal ions such as Pb^{2+}, Cu^{2+} and Cd^{2+} can be removed within 30 min and, after this period, the uptake of heavy metal ions remains almost unchanged with further increases of contact time. The adsorption of metal ions (Pb^{2+}, Cu^{2+} and Cd^{2+}) gradually increased with an increase of the pH of the medium, and maximum removal efficiency was observed at pH 6.2 (Figure 2B). They also observed the good chemical stability and reusability of these microspheres.

Sinha et al. [63] reported the adsorption of Cd, Pb, Hg and As metal ions by EDTA and thiol-functionalized (SH) γ-Fe$_2$O$_3$-incorporated mesoporous silica particles. They found that EDTA-functionalized magnetic mesoporous silica (MMS-EDTA) exhibited good performance for the removal of Cd and Pb, whereas SH-functionalized magnetic mesoporous silica (MMS-SH) exhibited a strong affinity for the removal of Hg and As. Bagheri et al. [64] have investigated the pH-dependent adsorption of Pb(II), Cd(II) and Cu(II) onto the iron oxide-silica magnetic particles with Schiff's base (Figure 2C). They studied the interference of coexisting ions on the recovery of metal ions (each metal ion at the 10 mg L^{-1} level) and found 95% recovery for the target analytes, even in the presence of 3 g L^{-1} K$^+$ and Na$^+$, 2 g L^{-1} Ca^{2+} and Mg^{2+}, 0.5 g L^{-1} NH$_4^+$, 0.1 g L^{-1} Fe^{3+}, 0.01 g L^{-1} Al^{3+}, Mn^{2+}, Co^{2+} and Ni^{2+}, 8 g L^{-1} SO$_4^{2-}$, 4 g L^{-1} Cl$^-$ and 6 g L^{-1} NO$_3^-$. They also investigated the presence of trace amounts of Pb(II), Cd(II) and Cu(II) ions in a wide variety of samples (tap water, petrochemical wastewater, tuna fish, shrimp, rice, tobacco and human hair) by using these Schiff's base modified iron oxide-silica magnetic particles.

Liu et al. [39] investigated the potential application of amine-functionalized magnetite chitosan nanocomposites as a recyclable tool for the removal of Pb^{2+}, Cu^{2+} and Cd^{2+}. They studied the adsorption/desorption mechanism of metal ions by these chitosan nanocomposites. The adsorption ability for the capture of Pb^{2+} onto nanocomposites was very fast (within 10 min). The removal efficiency of Pb^{2+} increased from 36.8% to 95.3% when the pH was changed from four to seven. They also reported on the effective removal of Pb^{2+} at above 93% and with up to six cycles.
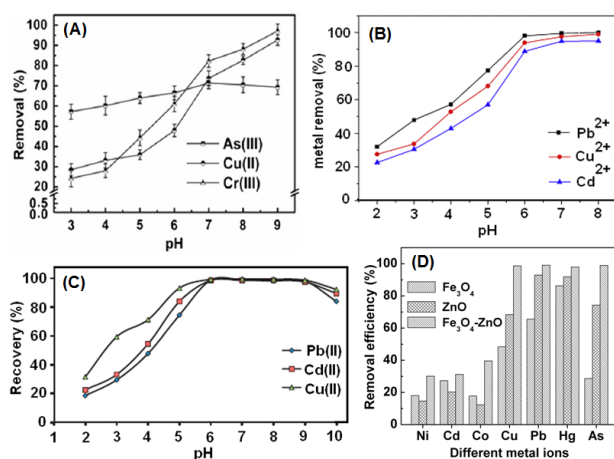

Figure 2. (A) Removal of 50 mg L^{-1} of As(III), Cu(II) and Cr(III) by 500 mg L^{-1} of Fe$_3$O$_4$–SiO$_2$-poly(1,2-diaminobenzene) at 30 ^{0}C [61]; (B) removal of Cu (II), Pb(II) and Cd(II) by Fe$_3$O$_4$@SiO$_2$@meso-SiO$_2$-NH$_2$ microspheres at different pHs [62]; (C) % recovery of metal ions by Fe$_3$O$_4$/SiO$_2$/Schiff base sorbent at different pHs [64]; and (D) removal of metal ions by Fe$_3$O$_4$, ZnO and Fe$_3$O$_4$-ZnO composites [40] (Reproduced with permission from [61,62, 64] copyright Elsevier and [40] copyright RSC publications).

Recently, Fe$_3$O$_4$-embedded ZnO magnetic semiconductor nanocomposites have also been explored for the simultaneous removal of various heavy metal ions (Ni^{2+}, Cd^{2+}, Co^{2+}, Cu^{2+}, Pb^{2+}, Hg^{2+} and As^{3+}) from wastewater (Figure 2D) [40]. The Fe$_3$O$_4$-embedded ZnO nanocomposite showed a much better removal efficiency for metal ions than Fe$_3$O$_4$ and ZnO individually. Interestingly, the complete removal of highly toxic metal ions, such as Cu^{2+}, Pb^{2+}, Hg^{2+} and As^{3+}, was achieved by these embedded nanocomposites. Further, it has been observed that these nanocomposites can be successfully used for the removal of Hg^{2+} at the ppb level. The list of Fe$_3$O$_4$, ZnO and TiO$_2$-based nanomaterials used for the removal of toxic metal ions is described in Table 1.

2.1.5. General mechanism of the removal of heavy metal ions

In order to understand the mechanism of the adsorption of metal ions by nanoparticles, a number of efforts have been undertaken in investigating the influence of the adsorption process using different techniques, such as infrared (IR) spectroscopy [65,66], X-ray diffraction (XRD) [5], X-ray photoelectron spectroscopy (XPS) [67] and extended X-ray absorption fine structure (EXAFS) spectroscopy [68]. The basis of discussion includes physical adsorption [67J, surface complexation [31], ion exchange [5], electrostatic interaction [31] and hard/soft acid-base interaction [31].
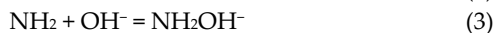
In general, the negatively-surface-charged nanoparticles form a chelate complex with metal ions above their point of zero charge (pzc) (i.e., pH > pHpzc). For example, the negatively-charged carboxylate ions (COO$^-$) of carboxyl - functionalized nanoparticles have a strong coordinative affinity in forming chelate complexes towards metal ions (M^{n+}) at pH>pHpzc. The enhanced chelation tendency of carboxylate ions at higher pHs is expected, as at lower pHs the chelation sites were occupied with H$^+$ (the chelation sites are neutral, i.e., -COOH) and were released at a higher pH, thereby originating the desired chelation. Also, at lower pHs, H$^+$ ions were adsorbed onto the surface of nanoparticles, leading to a net positive charge. A certain amount of metal ions can still be adsorbed by carboxyl-functionalized nanoparticles at pH < pH$_{pzc}$. This is perhaps due to the fact that ion exchange takes place at pH < pHpzc. Since the affinity of metal ions to Fe$_3$O$_4$ is higher than that of H$^+$ ions, metal ions can replace the adsorbed H$^+$ ions from the Fe$_3$O$_4$ surface by an ion exchange mechanism [5]. Liu et al. [29] observed the adsorption of metal ions - particularly Cd^{2+} - directly on the surface of Fe$_3$O$_4$ rather than on the coated organic moiety (humic acid). The adsorption of metal ions by ion exchange is relatively slow when as compared to surface complexation, since the organic molecules present on the surface of the nanoparticles may cause steric hindrance towards the adsorption of metal ions.

Catalysts	Metal ions	Working volume/ concentrations	Amount/ conditions	Efficiency (%)	Reference
Thiol-SiO$_2$@Fe$_3$O$_4$	**Hg^{2+}**	50 mL, 500 µg L^{-1}	0.40 mg, pH 4, 1 h	**97**	[26]
EDA-Fe$_3$O$_4$ polymers	**Cr^{6+}**	40 mL, 50 mg L^{-1}	50 mg, pH 2.5, 24 h	**99**	[27]
EDA-Fe$_3$O$_4$	Pb^{2+}	10 mg L^{-1}	15 mg, pH 7, 2 min	90	[28]
Humic acid-Fe$_3$O$_4$	Hg^{2+}, Pb^{2+}, Cd^{2+}, Cu^{2+}	100 mL, 0.1 mg L^{-1}	10 mg, pH 6, 15 min	**99 (Hg^{2+}, Pb^{2+}),** 95 (Cu^{2+}, Cd^{2+})	[29]
Ascorbic acid-Fe$_3$O$_4$	**As^{3+}, As^{5+}**	25 mL, 0.12 mg L^{-1}	5 mg, 24 h	**97.5 (All)**	[30]
DMSA-Fe$_3$O$_4$	Cr^{3+}, Co^{2+}, Ni^{2+}, Cu^{2+}, Cd^{2+}, Pb^{2+}, As^{3+}	40 mL, 10.17 Cr^{3+}, 15.75 Co^{2+}, 25.13 Ni^{2+}, 23.83 Cu^{2+}, 47.8 Cd^{2+}, 42.0 Pb^{2+}, 19.6 As^{3+} mg L^{-1}	50 mg, pH 8, 24 h,	97 (As^{3+}), **100 (Others)**	[31]
ZnO Nano-assembly	Co^{2+}, Ni^{2+}, Cu^{2+}, Cd^{2+}, Pb^{2+}, Hg^{2+} As^{3+}	40 mL, 15.75 Co^{2+}, 25.13 Ni^{2+}, 28.83 Cu^{2+}, 47.8 Cd^{2+}, 42 Pb^{2+}, 47.16 Hg^{2+}, 19.6 As^{3+} mg L^{-1}	50 mg, 24 h	**100 (Pb^{2+}, As^{3+}),** 7 (Cd^{2+}), 16 (Co^{2+}), 18 (Ni^{i2+}), 25 (Cu^{2+}), 64 (Hg^{2+})	[36]
Amine-Fe$_3$O$_4$@SiO$_2$	Pb^{2+}	50 mL, 300 mg L^{-1}	50 mg, pH 5.2, 16 h	89	[38]
Chitosan-Fe$_3$O$_4$ nanocomposites	**Pb^{2+}**	50 mL, 10 mg L^{-1}	15 mg, pH 4-7, 10 min	**95**	[39]
Fe$_3$O$_4$-ZnO	Co^{2+}, Ni^{2+}, Cu^{2+}, Cd^{2+}, Pb^{2+}, Hg^{2+}, As^{3+}	40 mL, 15.8 Ni^{2+}, 40 Cd^{2+}, 15.75 Co^{2+}, 23.83 Cu^{2+}, 36.22 Pb^{2+}, 45 Hg^{2+}, 22.55 As^{3+} mg L^{-1}	50 mg, pH 6, 24 h	**100 (Cu^{2+}, Pb^{2+}, Hg^{2+}, As^{3+}),** 40 (Co^{2+}), 22 (Cd^{2+}), 25 (Ni^{2+})	[40]
Glutaraldehyde– APTES-Fe$_3$O$_4$	Cu^{2+}	20 mL, 0.47 mM	25 mg, pH 5.3, 1 h	80	[48]
Fe$_3$O$_4$@APS@AA-co-CA Fe$_3$O$_4$	Pb^{2+}, Cu^{2+}, Cd^{2+}, Zn^{2+}	50 mL, 100 mg L^{-1}	50 mg, pH 4, 2 h	**100 (Pb^{2+}),** 95 (Cu^{2+}), 90 (Cd^{2+}), 88 (Zn^{2+})	[49]
Porous ZnO nano-plates	**Cu^{2+}**	100 mL, 2200 mg L^{-1}	5 mg, pH 4-6, 10 h	**100**	[52]
ZnO	Pb^{2+}, Cd^{2+}	100 mL, 200 mg L^{-1}	125 mg, 1 h	**96 (Pb^{2+}),** 91 (Cd^{2+})	[53]
TiO$_2$	**As^{3+}**	50 mL 3310 mg L^{-1}	1.5 g, pH 9, 24 h	**98**	[58]
Fe$_3$O$_4$–SiO$_2$-poly(1,2-diaminobenzene)	As^{3+}, Cu^{2+}, Cr^{3+}	100 mL, 50 mg L^{-1}	50 mg, pH 9, 2 h	97 (Cr^{3+}), 68 (As^{3+}), 92 (Cu^{2+})	[61]
Amine-Fe$_3$O$_4$@SiO$_2$@ meso-SiO$_2$	Pb^{2+}, Cu^{2+}, Cd^{2+}	50 mL 400 mg L^{-1}	50 mg, pH 6.2, 2 h	**99 (Pb^{2+}),** 95 (Cu^{2+}), 91 (Cd^{2+})	[62]
EDTA-γ-Fe$_3$O$_4$@SiO$_2$ /Thiol-γ-Fe$_3$O$_4$@SiO$_2$	**Cd^{2+}, Pb^{2+}, Hg^{2+}, As^{3+}**	1L, 1 mg L^{-1}	1 g, solution pH	**>97 (All)**	[63]
Fe$_3$O$_4$/SiO$_2$/Schiff base	**Pb^{2+}, Cd^{2+}, Cu^{2+}**	100 mL, 10 µg L^{-1}	150 mg, pH 7, 12 min	**100 (All)**	[64]

Table 1. Recent studies of metal ions removal using Fe$_3$O$_4$, ZnO and TiO$_2$-based nanomaterials at room temperature.

*The results (in bold letters) as shown above are the best removal efficiencies of metal ions at a particular pH.

www.intechopen.com

Sarika Singh, K. C. Barick and D. Bahadur: Functional Oxide Nanomaterials 7
and Nanocomposites for the Removal of Heavy Metals and Dyes

The mechanism for the sorption of metal ions by amine-functionalized nanoparticles can be expressed by the following reactions:

$$NH_2 + H^+ = NH_3^+ \qquad (1)$$
$$NH_2 + M^{n+} \rightarrow NH_2M^{n+} \qquad (2)$$
$$NH_2 + OH^- = NH_2OH^- \qquad (3)$$
$$NH_2OH^- + M^{n+} = NH_2OH^- \cdots M^{n+} \qquad (4)$$

The protonation of amine groups ($-NH_3^+$) and the surface complexation of metal ions ($-NH_2M^{n+}$) may occur simultaneously on the surface of nanoparticles at pH < pHpzc. However, only a few $-NH_2$ sites are available for the adsorption of metal ions through complexation due to the conversion of $-NH_2$ groups to $-NH_3^+$. Moreover, the electrostatic repulsion between M^{n+} and the nanoparticles increased with the formation of more $-NH_3^+$. All these effects would result in the reduction of M^{n+} adsorption on amine-functionalized nanoparticles at low pH. With increasing pH of solution (till pHpzc), H^+ concentration decreases and Eq. (1) proceeded to the left, leading to an increase of the number of NH_2 sites on the surface of amine-functionalized nanoparticles for M^{n+} adsorption through Eq. (2) and thus increasing the adsorption capacity [31,69]. However, the surface of amine-functionalized nanoparticles is negatively charged, due to the formation of $-NH_2OH^-$ at higher solution pH (pH > pHpzc) as shown in Eq. (3). This could reduce the adsorption of metal ions through complexation, but it might increase the adsorption of metal ions through the electrostatic attraction between NH_2OH^- and M^{n+}. Thus, the adsorption of metal ions by amine-functionalized nanoparticles increases with an increase of the pH of the solution.

In the case of thiol-functionalized nanoparticles, the adsorption mechanism of metal ions may involve two surface reactions, namely strong metal–sulphur complexation and weak electrostatic interaction. As anticipated from Pearson's hard/soft acid-base theory (HSAB) [70], the soft Lewis base (such as the thiol (SH) group) is the more favourable in undergoing a remarkable interaction with soft Lewis acids (heavy metal ions) rather than hard Lewis acids (alkali and alkaline earth metal ions). Thus, the thiol group (containing a soft donor atom, sulphur) on the surface of nanoparticles mainly reacts with heavy metal ions directly to form stable metal–sulphur complexes through chelation [23, 31]. In addition to the metal–sulphur complexation, Liang et al. [70] reported the non-specific adsorption of metal ions by thiol-functionalized nanoparticles through a less-selective electrostatic interaction between the metal ions and the oppositely charged surface functional groups at a certain distance from the surface.

The presence of organic ligands on the surface of nanoparticles and competing adsorbates can affect the removal efficiency of metal ions. Factors determining the effect that organic ligands have on metal ions adsorption include the type and concentration of the ligand and metal ion, the adsorbent type and the pH of the solution. In systems with more than one adsorbate, competition may occur among the adsorbates for surface sites. Generally, the degree of competition is dependent on the type and concentration of the competing ions, the number of surface sites and the affinity of the surface for the adsorbate. However, the adsorption process, followed by magnetic separation, leads to the rapid and inexpensive removal of metal ions.

2.2. Photocatalytic degradation of organic dyes

2.2.1 ZnO nanoparticles

Zinc oxide has received a great deal of attention in relation to the photocatalytic degradation of organic contaminants. It has been reported that different morphologies of ZnO exhibit different degrees of photocatalytic activity [16,33,72-78]. Ma et al. [72] and Zhai et al. [76] have reported on the photocatalytic activity of ZnO nano-rod arrays on arbitrary substrates and ZnO nano-disks in decomposing methyl orange (MO). Zheng et al. [77] investigated the photocatalytic activity of octahedron and rod-like porous ZnO architectures for the decomposing of MO in water under UV irradiation. Further, they noted the high catalytic efficiency of porous ZnO octahedron calcined at 500 ^{0}C rather than 700 ^{o}C due to their large surface area. Recently, the photodegradation of methylene blue (MB) and Rhodamine B (RhB) under UV light by different morphologies of ZnO architectures has also been investigated (Figure 3A) [78]. These include spherical assemblies (SAs), nano-rod assemblies (NRAs), cauliflower-like assemblies (CFAs) and mushroom-like assemblies (MAs). The complete removal of MB and RhB by CFAs was observed within 40 and 100 min of UV irradiation. These ZnO nanostructures were found to be good photocatalysts due to their mesoporous structure, high surface area and large amount of oxygen vacancy. The results showed that the photocatalytic activity of ZnO nanostructures is strongly dependent on the morphology of ZnO. Furthermore, these ZnO nanostructures have an excellent photocatalytic lifetime, and no significant loss of ZnO catalyst was observed up to the third cycle. Gupta et al. [16] have studied the photodegradation of MB over different-shaped ZnO nanostructures, observing that the photocatalytic activity is dependent on defect concentration.

There have been various reports on the enhancement of photocatalytic performance by doping impurities (Ag, Cu, I) [79-81]. Mohan et al. [80] demonstrated the photocatalytic activity of pure and Cu-doped ZnO nano-rods for the degradation of resazurin dye (Figure 3B). They

observed a significant enhancement of photocatalytic activity upon the doping of Cu into ZnO nano-rods. However, there are also reports on the suppression of the catalytic efficacy of ZnO nanostructures upon doping with transition metal ions [82-84]. Barick et al. [82] have observed a decrease in the photocatalytic activity of mesoporous ZnO nano-assemblies after doping with transition metal ions (Mn, Co and Ni) under UV light. Qiu et al. [83] also found that Co^{2+} doping markedly suppressed the photodegradation of RhB under UV irradiation. It is proposed that the substitutions of transition metal ions in a ZnO lattice may act as trapping or recombination centres for electrons and holes and, hence, substantially decrease the photodegradation efficiency. Ullah and Dutta [84] have reported the lower photodegradation efficiency of MB over Mn-doped ZnO as compared to pristine ZnO due to the faster recombination of electron–hole pairs following a change of the absorption characteristics caused by Mn^{2+} doping.

Furthermore, the amount of the catalyst [4,29], concentration of the dye [4], the pH of the medium [4] and time [72] all play a crucial role in photocatalytic degradation. The list of ZnO nanostructures that have been used to remove dyes under UV/visible light from wastewater is summarized in Table 2.
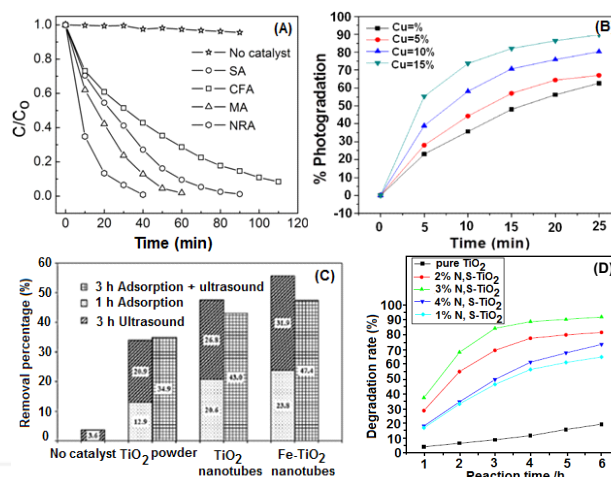

Figure 3. Photocatalytic degradation of: (A) MB with different nanostructures: spherical assemblies (SAs), nano-rod assemblies (NRAs), cauliflower-like assemblies (CFAs) and mushroom-like assemblies (MAs) of ZnO under UV light [78]; (B) resazurin by pure ZnO and Cu-doped ZnO photocatalyst with different Cu doping concentrations [80]; (C) dyes in the absence and presence of different TiO_2-based catalysts under ultrasonic irradiation [86]; and (D) MO by N- and S-doped TiO_2 with different contents at pH 4 under sunshine irradiation [107] (Reproduced with permission from [78] copyright RSC publications and [80,86,107] copyright Elsevier).

Catalyst (ZnO)	Dyes	Working volume/ concentrations	Amount/ conditions	Efficiency (%) with time	Reference
Nano-rods	MO	200 mL, 10 mg L^{-1}	50 mg, 250 W UV lamp	100, 60 min	[72]
Rod like ZnO	Rh6G	75 mL, 1× 10^{-5} M	7.5 mg, 12 W UV lamp	68, 100 min	[73]
Flower like ZnO	Phenol	50 mL, 12 mg L^{-1}	50 mg, 15 W UV lamp	100, 20 min	[75]
Nano-disks	MO	100 m L, 50 mg L^{-1}	20 mg, pH 3 UV light	100, 120 min	[76]
Porous octahedron	MO	5 mL, 10 mg L^{-1}	5 mg, 300 W Hg lamp	100, 20 min	[77]
Flower like assembly	MB, RhB	80 mL, 10 mg L^{-1}	24 mg, 25W, UV light	100, 40 min and 100 min respectively	[78]
1% Ag-doped ZnO	MO	50 mL, 1 mg mL^{-1}	50 mg, 100 W UV lamp	100, 60 min	[79]
Cu-doped ZnO	Resazurin	10 mL, 1.5 mg L^{-1}	0.1 mg, UV light	90, 20 min	[80]
Mn doped ZnO Nano-assembly	MB	80 mL, 10 mg L^{-1}	24 mg, 25 W UV light	40, 90 min	[82]
Co doped ZnO	RhB	100 mL, 10^{-5} M	80 mg, 6 W UV & 300 W halogen lamp	100, 5 h and 100, 24 h	[83]

Table 2. Room temperature catalytic studies on the removal of dyes with ZnO under UV/visible light.

Catalyst (TiO$_2$)	Dyes	Working volume/ concentrations	Amount/conditions	Efficiency (%), with time	Reference
Ag-doped TiO$_2$	Toluene	2 L, 9.0 mg L^{-1}	1.5 g, 28 W UV lamp	71, 210 min	[88]
Nd doped TiO$_2$	MB	60 mL, 10 mg L^{-1}	30 mg, pH 3, 150 W, UV lamp	100 120 min	[89]
10 wt% MgO doped TiO$_2$	4-chlorophenol	50 mL, 25 mg L^{-1}	100 mg, 16 W UV lamp, pH 5.2	100, 60 min	[90]
Bi & B Co-doped TiO$_2$	AO7, 2, 4-DCP	60 mL, 20 mg L^{-1}	60 mg, 1000 W tungsten halogen lamp	25, 240 min and 100, 240 min	[91]
Gd doped TiO$_2$	MO	150 mL, 0.02 g L^{-1}	300 mg, Xe-lamp	97.3, 150 min	[92]
PANI/TiO$_2$	MB RB	50 mL, 10^{-5} mol L^{-1}	50 mg, 300 W, sun light	60, 6 h and 100, 6 h, respectively	[93]
C-doped TiO$_2$ at 200 ^{0}C	Toluene	1.8 L, 150 mg m^{-3}	200 mg, 150 W Xe lamp	60, 120 min	[94]
C-doped TiO$_2$ at 500 ^{0}C	Toluene	1.8L, 150 mg m^{-3}	200 mg, 150 W Xe lamp, solar light	100, 20 min	[95]
C-self-doped TiO$_2$ sheets	MB	25 mL, 2x10^{-5} M	100 mg, 350 W Xe lamp, visible light	100, 120 min	[97]
N-TiO$_2$ at 500 °C	MB, 4-chlorophenol	50 mL, 10^{-5} M & 10 mg L^{-1}	60 mg, 25 mg, 60 W house-bulb	100, 300 min & 100, 120 min	[98]
N-doped TiO$_2$	MB	30 mL, 10^{-5} M	12.5 mg, 1000 W, Xe lamp	100, 200 min	[99]
N doped TiO$_2$	Phenol	20 mL, 50 mg L^{-1}	20 mg, 350 W Xe arc lamp	65, 120 min	[100]
N-doped TiO$_2$	Lindane	200 mL, 3.44×10^{-4} mmol L^{-1}	50 mg, 500 W visible lamp, pH 5–9	100, 330 min	[101]
C–N co-doped rod-like TiO$_2$	MB	300 mL, 10 mg L^{-1}	50 mg, 500 W Xe lamp	100, 180 min	[103]
B-doped TiO$_2$	MB	200 mL, 10 mgL^{-1}	50 mg, 300 W Xe-lamp	84, 60 min	[104]
C, S, N and Fe-doped TiO$_2$	RhB	100 mL, 10^{-5} mol L^{-1}	30 mg, 1000 W Hg lamp, visible light	100, 150 min	[106]
N, S-TiO$_2$, 500 °C	MO	400 mL, 10 mg L^{-1}	400 mg, pH 4, sunshine	92, 360 min	[107]

Table 3. Room temperature catalytic studies on the removal of dyes with TiO$_2$ under UV/visible light.

2.2.2 TiO$_2$ nanoparticles

Titanium dioxide is another highly favourable material for heterogeneous photocatalytic processes due to its high photoactivity, non-toxic nature, large band-gap and stability. There have been numerous reports on the photoabsorption and photocatalytic properties of TiO$_2$ under UV light [85-88]. Xie et al. [85] have studied the photocatalytic activity of TiO$_2$ at three different temperatures (120, 160 and 200 ^{0}C) and found the highest activity at 160 ^{0}C. They also doped TiO$_2$ with Si and observed that Si doping does not improve the photocatalytic activity of TiO$_2$. However, it has been reported that the photocatalytic activity of TiO$_2$ can be enhanced, either by doping with transition metal ions (Fe, Bi, Ag and V) and rare-earth metal ions (Nd, Gd), or by the surface modification of the crystalline structure, as they could significantly influence charge carrier recombination rates and interfacial electron-transfer rates [82-89]. Pang et al. [86] have demonstrated that Fe-doped TiO$_2$ nanotubes are an efficient candidate for the purification of real textile wastewater containing a mixture of organic dyes (which included reactive, vat and disperse dyes) as compared to TiO$_2$ powder and TiO$_2$

nanotubes (Figure 3C). Similar results were also observed by Bzdon et al. [87] in relation to the decomposition of sodium dodecylbenzene sulphonate by Fe-doped TiO2. Li et al. [88] have demonstrated the use of Ag-doped TiO2 for the degradation of toluene. They reported that the photodegradation of toluene increases with an increase of the concentration of Ag doping in TiO2 under visible light, whereas an irregular trend was observed under UV light. The enhancement of the visible light photocatalytic activity of TiO2 with the doping of non-metallic elements, such as carbon (C), nitrogen (N), boron (B) and sulphur (S) has also been reported in the literature [87-107]. Yu et al. [97] have reported on the complete photodegradation of MB after 120 min by carbon self-doped TiO2 sheets under visible light. Ju et al. [107] have also observed a higher catalytic activity of 3% for N- and S-doped TiO2 nanoparticles in the degradation of MO at pH 4 under sunshine irradiation (Figure 3D). Table 3 lists the representative studies on the UV/visible light-induced photodegradation of organic dyes using TiO2 nanoparticles.

2.2.3 ZnO and TiO2-based oxide nanocomposites

Recently, various kinds of ZnO and TiO2-based nanocomposites were developed for the enhancement of the photocatalytic degradation of organic dyes. For instance, a large number of binary and ternary nanocomposites of ZnO and TiO2, such as ZnO/TiO2 [108-111], chitosan–polyaniline/ZnO hybrid [112], ZnO/ TiO2-metal (Ag, Au) composites [113-116], N-doped TiO2/C [117], B-doped Au/TiO2 [118], Ag@SiO2@TiO2 core shell [41,119], TiO2@C/Ag [120], TiO2/ZnO/Au [121] and TiO2−AgBr−Ag [122,123], with well-defined structures, have been explored for the photodegradation of organic dyes. Liu et al. [41] have investigated the photocatalytic activity of TiO2–SiO2–Ag ternary nanocomposites, demonstrating that the photocatalytic activity of these ternary nanocomposites was higher than that of TiO2–Ag, TiO2–SiO2, TiO2 and their physical mixture (Figure 4A). They also investigated the coexistence of the optimum amount SiO2 and Ag in TiO2 for the enhancement of photocatalytic performance under visible light irradiation. They demonstrated that the higher catalytic efficiency of TiO2–SiO2–Ag in the degradation of RhB is due to the interaction between Si−OH and the carboxylic groups of RhB through a monodentate ester-like linkage. Zhang et al. [121] also studied the photocatalytic efficiency of Au-embedded TiO2/ZnO nanofibres for the photodegradation of MO and 4-nitrophenol. Their results showed that the efficiency of this embedded nanocomposite is 96% for the degradation of MO and 4-nitrophenol after 30 and 40 min, respectively, as compared to pure TiO2, ZnO and TiO2/ZnO nanofibres under ultraviolet excitation, due to separation of photo-generated electron-hole pairs based on a synergistic

heterostructure among the TiO2, ZnO and Au (Figure 4B). Their stability test of Au/TiO2/ZnO showed that it is easily recycled for reuse. Recently, Tang et al. [123] demonstrated the visible light photocatalytic activity of Ag/AgX/TiO2 hybrid nanostructures (X= Cl, Br, I) for the decomposition of MO, and compared their efficacy with a pure titanate nano-wired honeycomb like-structure (Figure 4C). They also found a higher efficiency with an Ag/AgCl/TiO2 hybrid as compared to Ag/AgBr/TiO2 and Ag/AgI/TiO2, and it completely degraded the MO within 160 min whereas the pure TiO2 nano-wired honeycomb did not show any catalytic performance. They attributed the higher catalytic efficiency of the Ag/AgCl/TiO2 composite to the combined effect of the surface plasmon of Ag nanoparticles and the electron/hole separation by the metal/ semiconductor structure.
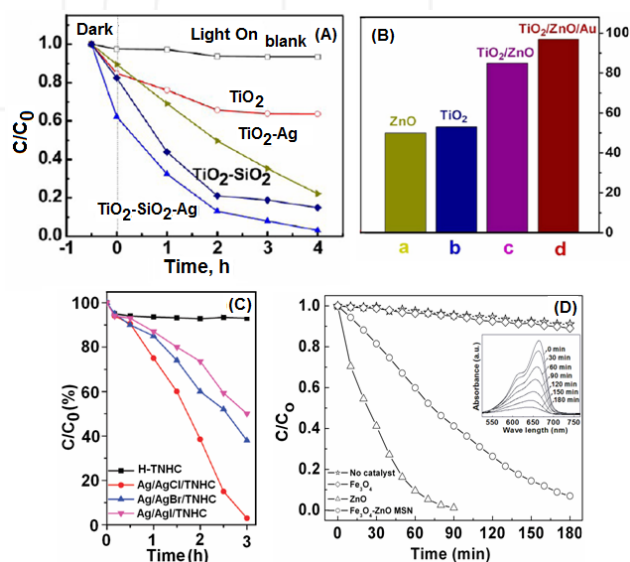

Figure 4. Photocatalytic degradation of: (A) RhB without any catalyst and with TiO2, TiO2–Ag, TiO2–SiO2 and TiO2–SiO2–Ag as the catalysts under visible light [41]; (B) MO over different catalysts for 30 min under UV light [121]; (C) MO by different silver/silver halides/titanate films under visible light illumination [123]; and (D) MB in the presence and absence of nano-adsorbents (inset shows the time-dependent absorption spectra of MB degradation over Fe3O4–ZnO [40] (Reproduced with permission from [41,123] copyright American Chemical Society Publications; [121] copyright Elsevier and [40] copyright RSC publications).

Recently, magnetic photocatalysts have emerged as new materials for environmental decontamination, being highly efficient, separable and reusable materials for the removal of contaminants from a solution via an external magnetic field [26,40,124-128]. Nabid et al. [128] have prepared a highly efficient TiO2/ZnO/Fe3O4/PANI visible light photocatalyst and investigated their use in the photocatalytic degradation of MO. It is important to mention that the TiO2/ZnO/Fe3O4/PANI composite shows much higher catalytic activity as compared to ZnO/Fe3O4/PANI, TiO2/Fe3O4/PANI, TiO2/ZnO, ZnO/Fe3O4,

TiO₂/ZnO/Fe₃O₄ and their individual counterparts. Further, they have observed that the degradation efficiency of MO remained over 70% after 10 generations. A novel recyclable and magnetically-separable Fe_3O_4–ZnO nanocomposite was also developed for the degradation of MO and RhB under UV light (Figure 4D) [40]. In brief, all these studies demonstrated that stable magnetic semiconductor nanocomposites can serve as good photocatalysts for the degradation of organic contaminants. Furthermore, they can be separated easily by an external magnet and reused several times. The lists of ZnO and TiO₂-based nanocomposites used for the photodegradation of organic dyes under UV/visible light is described in Table 4.

2.2.4. Other oxide-based nanocomposites

Besides TiO₂ and ZnO, there are also many other semiconductors and their nanocomposites, such as $BiVO_4/CuCr_2O_4$ [129], $TiO_2/(ZnS)_x(CuInS_2)_{1-x}$ [130], Bi_2WO_6 [131], Ag_3PO_4/TiO_2 [132], Ag_2CO_3 [133] and $Bi_2TiO_4F_2$ [134], which have been reported as having excellent photocatalytic properties under visible light.

Recently, Bajaj et al. [129] have demonstrated the use of $BiVO_4/CuCr_2O_4$ nanocomposites as a visible light photocatalyst for the degradation of MB dye (Figure 5A). They found a 90% degradation efficiency by $BiVO_4/CuCr_2O_4$ nanocomposites with a 1:0.25 ratio in 180 min, which is three-times higher than their individual counterparts. Further, they also observed the enhancement in the degradation efficiency (95%) upon the addition of polyaniline with a 1:1 ratio. A new high-efficiency visible light photocatalyst, Ag_2CO_3, has been developed by Dong et al. [133] with an ion-exchange method (Figure 5B). This research group reported the excellent photocatalytic activity of Ag_2CO_3 in the absence and presence of radical scavengers (DMSO and benzoquinone) for the degradation of RhB, MO and MB dyes under visible light. The list of other nanocomposites used for degradation of dyes under visible light is summarized in Table 5.
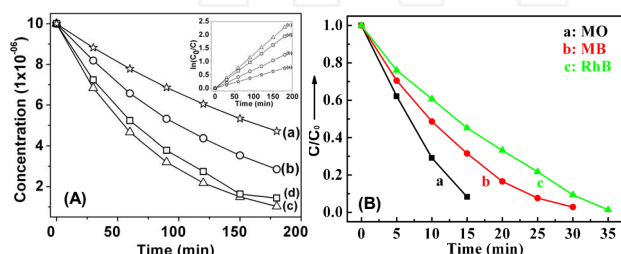

Figure 5. Photocatalytic degradation efficiency of: (A) MB using bare BiVO₄ (a) and BiVO₄/CuCr₂O₄ composites with ratio of 1:1 (b), 1:0.25 (c) and 1:0.0625 (d) (inset of figure shows their respective kinetic fit curves for dye degradation) [129]; and (B) MO, MB and RhB with Ag₂CO₃ under visible light illumination with 400 nm [133] (Reproduced with permission from [129] copyright RSC publications and [133] copyright from Elsevier).

2.2.5. General mechanism of photocatalysis

Semiconductor photocatalysis is based on the generation of an electron-hole (e⁻-h⁺) pair upon UV/visible light irradiation. The light of the energy is greater than the band-gap of the semiconductor nanoparticles and can excite an electron from the valence band to the conduction band (e⁻_CB), leaving behind a hole (h⁺_VB) in the valence band [75,135]. If the charge separation is maintained, the electron and the hole might migrate to the semiconductor surfaces, where they participate in redox reactions with the adsorbed organic species [16]. The defect sites may work as electron acceptors during the process of photocatalytic reaction and trap the photo-generated electrons, temporarily, so as to reduce the surface recombination of electrons and holes. The electrons in the conduction band can be rapidly trapped by molecular oxygen adsorbed on the nanoparticle, which is reduced to form a superoxide radical anion ($O_2^{•-}$). The holes can react with water adhering to the surface of the nanoparticles to produce •OH radicals, which are powerful oxidants. These reactive oxygen species ($O_2^{•-}$, •OH and H_2O_2) can subsequently oxidize organic dyes with mineralization-producing mineral salts, CO₂ and H₂O. The schematic representation of the photocatalytic process on the surface of semiconductor nanoparticles is shown in Figure 6.
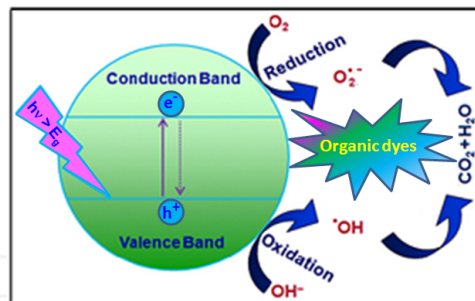

Figure 6. Schematic representation of the photocatalytic process on the surface of semiconductor nanoparticles.

It has been observed that the nano-particulates of ZnO and TiO₂, as well as their nanocomposites, are an excellent photocatalyst for the degradation of organic dyes under the irradiation of UV light. These nanostructures exhibit higher photocatalytic activity than their bulk counterparts. However, an efficient photocatalytic process requires the suppression of electron–hole recombination by trapping the charge carriers at the defect states. Thus, photocatalytic activity can be enhanced, either by the presence of inherent defect states related to shape, size and morphology, or by intentionally-created defect states within the band-gap through doping with transition metal ions. Furthermore, various oxide-based visible light photocatalysts are developed for the degradation of organic dyes.

Catalyst (Nanocomposites)	Dyes	Working volume/ concentrations	Amount, conditions	Efficiency (%), with time	Reference
TiO$_2$/ZnO nanofibres, 650 ^{0}C	RhB	1L, 10^{-6} M	1 g, 300 W tungsten halogen lamp	100, 75 min	[108]
TiO$_2$@ZnO n–p-n heterojunction nano-rods	MO	100 mL, 20 mg L^{-1}	10 mg, 300 W UV lamp	80, 60 min	[110]
ZnO/TiO$_2$ coupled oxide	MO	1L, 20 mg L^{-1}	2.5 g, 125 W Hg lamp	100, 23 min	[111]
Chitosan–polyaniline/ZnO hybrid	Reactive orange 16	50 mL, 25 mg L^{-1}	25 mg, pH 5.8, 15 W UV lamp	99.8, 50 min	[112]
Ag@TiO$_2$ nanocomposite	MB	25 mL, 10 mg L^{-1}	0.5 mM, 400 W visible lamp	97, 240 min	[113]
Ag@TiO$_2$	RhB	20 mL, 1×10^{-5} M	50 mg, 300W Xe UV-lamp	100, 60 min	[114]
Au-TiO$_2$ nanotubes array	MO	200 mL, 5 mg L^{-1}	1.14 wt %, 150 W Xe arc lamp, pH 7	100, 150 min	[115]
4% Au-ZnO	Rh6G	50 mL, 10 mg L^{-1}	50 mg, Hg lamp UV-light	87, 450 min	[116]
N-doped TiO$_2$/C nanocomposites	MO	50 mL, 15 mgL^{-1}	50 mg, 500 W Xe lamp	100, 120 min	[117]
Au/B/TiO$_2$	MB	1L, 12.5 mg L^{-1}	1.0 g, visible light	60, 120 min	[118]
TiO$_2$–SiO$_2$–Ag nanocomposites	RhB	50 mL, 10 mg L^{-1}	50 mg, 150 W Xe lamp, visible light	100, 240 min	[41]
Ag@SiO$_2$@TiO$_2$	MB	150 mL, 2.0x10^{-5} M	50 mg, 150 W Xe lamp, visible light	100, 300 min	[119]
TiO$_2$@C/Ag nanofibres	RhB, MB	100 mL, 5 mg L^{-1}	30 mg, 150 W, Xe lamp, visible light	91, 6 h and 90, 7 h, respectively	[120]
TiO$_2$/ZnO/Au nanofibres	MO	100 mL, 10 mg L^{-1}	10 mg, 50 W Hg lamp, UV light	96, 30 min	[121]
Ag/AgCl/TiO$_2$ thin film	MO	20 mL, 5 mg L^{-1}	300 W Xe lamp, visible light	100, 180 min	[123]
AgBr-TiO$_2$/ SiO$_2$@Fe$_3$O$_4$	MB	120 mL, 10 mg L^{-1}	200 mg, 500 W Xe lamp, visible light	79, 90 min	[124]
Fe$_3$O$_4$/hydroxyl-apatite	Diazinon	1L, 10 mg L^{-1}	4.0 g, pH 5.5, 30 W Hg lamp, UV light	75, 60 min	[125]
Fe$_3$O$_4$/ZnO nanocomposites	MO	60 mL, 6×10^{-5} mol L^{-1}	30 mg, pH 7, 500 W Hg lamp	93.6, 60 min	[126]
Fe$_3$O$_4$/SiO$_2$/TiO$_2$ composites	RhB	50 mL, 1.0x10^{-5} M	25 mg, 15 W UV lamp	100, 40 min	[127]
TiO$_2$/ZnO/Fe$_3$O$_4$/ PANI	MO	100 mL, 10 mg L^{-1}	75 mg, pH >7 22 W visible light	97, 25 min	[128]

Table 4. Room temperature catalytic studies on the removal of dyes with ZnO- and TiO$_2$-based nanocomposites under UV/visible light.

www.intechopen.com

Sarika Singh, K. C. Barick and D. Bahadur: Functional Oxide Nanomaterials 13 and Nanocomposites for the Removal of Heavy Metals and Dyes

Catalyst (Nanocomposites)	Dyes	Working volume/ concentrations	Amount/ conditions	Efficiency (%), with time	Reference
$BiVO_4/CuCr_2O_4/PANI$	MB	40 mL, 10 mg L^{-1}	10 mg, 65 W, Philips lamp	95, 20 min	[129]
Ag_3PO_4/TiO_2	MB, RhB	100 mL, 20 mg L^{-1}	50 mg, 300 W Xe arc lamp	90, 42 min & 6, 42 min	[132]
Ag_2CO_3	RhB MO MB	100 mL, 10 mgL^{-1}	300W Xe arc lamp, visible light	100, 35 min 90, 15 min & 95, 30 min, respectively	[133]
$Bi_2TiO_4F_2$-12 h	RhB	60 mL, 10 mgL^{-1}	50 mg, 300 W Xe lamp	100, 150 min	[134]

Table 5. Other oxides nanocomposites for the degradation of dyes under visible light at room temperature.

3. Summary and future scope

Environmental pollution by toxic metal ions and organic contaminants is a global menace and its magnitude is increasing significantly. The recent development of nanotechnology offers great scope for the fabrication of desired nanomaterials with large surface-to-volume ratios and unique surface functionalities in treating these pollutants. Specifically, oxide-based nanomaterials, such as Fe_3O_4, ZnO and TiO_2, as well as their nanocomposites, show great potential for the removal of toxic metal ions and organic pollutants from contaminated water. These nanomaterials are generally modified with different functional groups to improve their catalytic efficiency and lifetime. Further, the use of magnetic nanomaterials or their nanocomposites provides the feasibility of magnetic separation and reusability (not possible with non-magnetic nanomaterials), which are significant for practical application. This article provides a comprehensive review of these oxide-based nanomaterials for water purification. However, the research in this area is in its nascent stage, and detailed investigations are required to establish the large-scale purification of water in real life.

In future, researchers should focus on the development of novel nanomaterials/nanocomposites with a high surface area, sufficient surface functional groups and high sorption ability, for the removal of different heavy metal ions and organic dyes. The microbial threats to human health and safety are also a serious public concern. Thus, further improvements must be made in the direction of the development of materials with greater stability (resistance to pH changes and concentrations of chemicals present in contaminated water) and the capacity for the simultaneous removal of multiple contaminants, such as toxic metal ions, organic dyes and bacterial pathogens. Considering the economics of adsorbents, it is necessary to synthesize low-cost, effective and recyclable adsorbents for their extensive application in our daily life. In addition, a wide range of treatment technologies should be developed for the purification of water in order to meet the demand of increased environmental pollution.

5. References

[1] Environmental Protection Agency, US Environmental protection agency report DC, (2007) EPA100/B-07/001, EPA Washington.

[2] Rajkumar D and Jong G K (2006) Oxidation of various reactive dyes with in situ electro-generated active chlorine for textile dyeing industry wastewater treatment. J. Hazard. Mater. B. 136: 203–212.

[3] Gómez-Álvarez A, Valenzuela-García J L, Meza-Figueroa D, De la O-Villanueva M, Ramírez-Hernández J, Almendariz-Tapia J, Pérez-Segura E (2011) Impact of mining activities on sediments in a semi-arid environment: San Pedro River, Sonora, Mexico. Appl. Geochem. 26: 2101–2112.

[4] Kansal S K, Singh M and Sud D (2007) Studies on photodegradation of two commercial dyes in aqueous phase using different photocatalysts. J. Hazard. Mater. 141: 581–590.

[5] Shen Y F, Tang J, Nie Z H, Wang Y D, Ren Y and Zuo L (2009) Preparation and application of magnetic Fe_3O_4 nanoparticles for wastewater purification. Sep. Purif. Technol. 68: 312–329.

[6] Smith A H, Lingas E O and Rahman M (2000) Contamination of drinking-water by arsenic in Bangladesh: a public health emergency, Bulletin of the World Health Organization. 78: 1093-1103.

[7] Henretig F M (2006) In: Goldfrank's Toxicologic Emergencies (Flomenbaun N E, Goldfrank L R, Hoffman R S, Howland M A, Lewin N A, Nelson L S,

eds). 8th edition, New York: McGraw-Hill, 1308–1324; Lead.

[8] Borba C E, Guirardello R, Silva E A, Veit M T and Tavares C R G (2006) Removal of nickel (II) ions from aqueous solution by biosorption in a fixed bed column: experimental and theoretical breakthrough curves. Biochem. Eng. J. 30: 184-191.

[9] Bull S (2011) HPA Compendium of Chemical Hazards Inorganic mercury/ elemental mercury. CRCE HQ, HPA (Version 3). http://www.hpa.org.uk/webc/HPAwebFile/HPAweb_C/1194947406874.

[10] Kazantzis G and Blanks R (1992) A mortality study of cadmium exposed workers. In: Edited Proceedings of the Seventh International Cadmium Conference, New Orleans. 150-157. London: Cadmium Association. 1992.

[11] Reife A and Fremann H S (1996) Environmental chemistry of dyes and pigments. John Wiley & Sons Inc, New York.

[12] Chen S, Zou Y, Yan Z, Shen W, Shi S, Zhang X and Wang H (2009) Carboxymethylated-bacterial cellulose for copper and lead ion removal. J. Hazard Mater. 161: 1355–1359.

[13] Chen Y, Pan B, Li H, Zhang W, Lv L and Wu J (2010) Selective removal of Cu (II) ions by using cation-exchange resin-supported polyethyleneimine (PEI) nanoclusters. Environ. Sci. Technol. 44: 3508–3513.

[14] Maliyekkal S M, Lisha K P and Pradeep T (2010) A Novel cellulose-manganese oxide hybrid material by in situ soft chemical synthesis and its application for the removal of Pb (II) from Water. J. Hazard. Mater. 181: 986–995.

[15] Xu F, Zhang N, Long Y, Si Y, Liu Y, Mi X, Wang X, Xing F, You X and Gao J (2011) Porous CS monoliths and their adsorption ability for heavy metal ions. J. Hazard. Mater. 188: 148–155.

[16] Gupta J, Barick K C and Bahadur D (2011) Defect mediated photocatalytic activity in shape-controlled ZnO nanostructures. J. Alloys Compd. 509: 6725–6730.

[17] Song J, Oh H, Kong H and Jang J (2011) Polyrhodanine modified anodic aluminum oxide membrane for heavy metal ions removal. J. Hazard. Mater. 187: 311–317.

[18] Jang S H, Jeonga G Y, Mina B G, Lyoob, W S and Lee S C (2008) Preparation and lead ion removal property of hydroxyapatite/polyacrylamide composite hydrogels. J. Hazard. Mater. 159: 294–299.

[19] Ambashta R D and Sillanpää M (2010) Water purification using magnetic assistance: A review. J. Hazard. Mater. 180: 38–49.

[20] Kamat P V, Huehn R and Nicolaescu R (2002) A "Sense and Shoot" Approach for Photocatalytic Degradation of Organic Contaminants in Water. J. Phys. Chem. B. 106: 788-794.

[21] Ivanov V, Tay J H, Tay S T and Jiang H L (2004) Removal of micro-particles by microbial granules used for aerobic wastewater treatment. Water Sci. Technol. 50: 147–154.

[22] Hillie T, Munasinghe M, Hlope M, Deraniyagala Y (2006) Nanotechnology, water and development. Meridian Institute. 1–44.

[23] Yantasee W, Warner C L, Sangvanich T, Addleman R S, Carter G T, Wiacek R J, Fryxell G E, Timchalk C and Warner M G (2007) Removal of heavy metals from aqueous systems with thiol functionalized superparamagnetic nanoparticles. Environ. Sci. Technol. 41: 5114-5119.

[24] Xu F, Zhang P, Navrotsky A, Yuan Z-Y, Ren T-Z, Halasa M and Su B-L (2007) Hierarchically assembled porous ZnO nanoparticles: Synthesis, surface energy, and photocatalytic activity. Chem. Mater. 19: 5680–5686.

[25] Feng J, Zhang D-D, Liu Y-F, Bai Y, Chen Q-D, Liu S-Y and Sun H-B (2010) Magnetic nanofilm of Fe_3O_4 for highly efficient organic light-emitting devices. J. Phys. Chem. C. 114: 6718–6721.

[26] Hakami O, Zhang Y and Banks C J (2012) Thiol-functionalised mesoporous silica-coated magnetite nanoparticles for high efficiency removal and recovery of Hg from water. Water Research. 46: 3913–3922.

[27] Zhao Y -G, Shen H -Y, Pan S -D and Hu M -Q (2010) Synthesis, characterization and properties of ethylenediamine-functionalized Fe_3O_4 magnetic polymers for removal of Cr(VI) in wastewater. J. Hazard. Mater. 182: 295–302.

[28] Wang L, Li J, Jiang Q and Zhao L (2012) Water-soluble Fe_3O_4 nanoparticles with high solubility for removal of heavy-metal ions from waste water. Dalton Trans. 41: 4544–4551.

[29] Liu J F, Zhao Z S, Jiang G B (2008) Coating Fe_3O_4 Magnetic nanoparticles with humic acid for high efficient removal of heavy metals in water. Environ. Sci. Technol. 42: 6949–6954.

[30] Feng L, Cao M, Ma X, Zhu Y and Hu C (2012) Superparamagnetic high-surface-area Fe_3O_4 nanoparticles as adsorbents for arsenic removal. J. Hazard. Mater. 217–218: 439–446.

[31] Singh S, Barick K C and Bahadur D (2011) Surface engineered magnetic nanoparticles for removal of toxic metal ions and bacterial pathogens. J. Hazard. Mater. 192: 1539–1547.

[32] Hu J-S, Zhong L-S, Song W-G and Wan L-J (2008) Synthesis of hierarchically structured metal oxides and their application in heavy metal removal. Adv. Mater. 20: 2977–2982.

[33] Li B and Wang Y (2010) Facile Synthesis and enhanced photocatalytic performance of flower-like ZnO hierarchical microstructures. J. Phys. Chem. C. 114: 890–896.

www.intechopen.com

Sarika Singh, K. C. Barick and D. Bahadur: Functional Oxide Nanomaterials and Nanocomposites for the Removal of Heavy Metals and Dyes   15

[34] Wang X, Cai W, Liua S, Wang G, Wu Z and Zhao H (2013) ZnO hollow microspheres with exposed porous nanosheets surface: structurally enhanced adsorption towards heavy metal ions. Colloids Surf. A: Physicochem. Eng. Aspects. 422: 199–205.

[35] Visa M, Carcel R A, Andronic L and Duta A (2009) Advanced treatment of wastewater with methyl orange and heavy metals on TiO_2, fly ash and their mixtures. Catalysis Today. 144: 137–142.

[36] Singh S, Barick K C and Bahadur D (2011) Novel and efficient three dimensional mesoporous ZnO nanoassemblies for environmental remediation. Int. J. Nanosci. 10: 1001-1005.

[37] Parida K, Krushna Mishra G and Dash S K (2012) Adsorption of toxic metal ion Cr(VI) from aqueous state by TiO_2-MCM-41: Equilibrium and kinetic studies, J. Hazard. Mater. 241– 242: 395–403.

[38] Zhang J, Zhai S, Li S, Xiao Z, Song Y, Ana Q and Tian G (2013) Pb(II) removal of $Fe_3O_4@SiO_2$–NH_2 core–shell nanomaterials prepared via a controllable sol–gel process. Chem. Eng. J. 215–216: 461–471.

[39] Liu X, Hu Q, Fang Z, Zhang X and Zhang B (2009) Magnetic chitosan nanocomposites: A useful recyclable tool for heavy metal ion removal. Langmuir. 25: 3-8.

[40] Singh S, Barick K C and Bahadur D (2013) Fe_3O_4 embedded ZnO nanocomposites for the removal of toxic metal ions, organic dyes and bacterial pathogens. J. Mater. Chem. A. 1: 3325-3333.

[41] Liu C, Yang D, Jiao Y, Tian Y, Wang Y and Jiang Z (2013) Biomimetic synthesis of TiO_2–SiO_2–Ag nanocomposites with enhanced visible-light photocatalytic activity. ACS Appl. Mater. Interfaces. 5: 3824–3832.

[42] Fu F and Wang Q (2011) Removal of heavy metal ions from wastewaters: a review. J. Environ. Manag. 92: 407-418.

[43] Shen Y F, Tang J, Nie Z H., Wang Y D, Ren Y and Zuo L (2009) Preparation and application of magnetic Fe_3O_4 nanoparticles for wastewater purification. Sep. Purif. Technol. 25: 312–319.

[44] Yavuz C T, Mayo J T, Yu W W, Prakash A, Falkne J C, Yean S, Cong L, Shipley H J, Kan A, Tomson M, Natelson D and Colvin V L (2006) Low-field magnetic separation of monodisperse Fe_3O_4 nanocrystals. Science. 314: 964–967.

[45] Yean S, Cong L, Yavuz C T, Mayo J T, Yu W W, Kan A T, Colvin V L and Tomson M B (2005) Effect of magnetite particle size on adsorption and desorption of arsenite and arsenate. J. Mater. Res. 20: 3255-3266.

[46] Mayo J T, Yavuz C, Yean S, Cong L, Shipley H, Yu W, Falkner J, Kan A, Tomson M, Colvin V L (2007) The effect of nanocrystalline magnetite size on arsenic removal. Sci. Technol. Adv. Mater. 8: 71–75.

[47] Singh S, Barick K C and Bahadur D (2013) Nanomagnetic chelators for removal of toxic metal ions. AIP Conf. Proc. 1512: 440–441.

[48] Ozmen M, Can K, Arslan G, Tor A, Cengeloglu Y and Ersoz M (2010) Adsorption of Cu(II) from aqueous solution by using modified Fe_3O_4 magnetic nanoparticles. Desalination. 254: 162–169.

[49] Ge F, Li Meng-Meng, Ye H and Zhao Bao-Xiang (2012) Effective removal of heavy metal ions Cd^{2+}, Zn^{2+}, Pb^{2+}, Cu^{2+} from aqueous solution by polymer-modified magnetic nanoparticles. J. Hazard. Mater. 211– 212: 366–372.

[50] Wang Z, Wub D, Wub G, Yang N and Wua A (2013) Modifying Fe_3O_4 microspheres with rhodamine hydrazide for selective detection and removal of Hg^{2+} ion in water. J. Hazard. Mater. 244–245: 621–627.

[51] Warner C L, Addleman R S, Cinson A D, Droubay T C, Engelhard M H, Nash M A, Yantasee W and Warner M. G (2010) High-performance, superparamagnetic, nanoparticle-based heavy metal sorbents for removal of contaminants from natural waters. Chem. Sus. Chem. 3: 749–757.

[52] Wang X B, Cai W P, Lin Y X, Wang G Z and Liang C H (2010) Mass production of micro/nanostructured porous ZnO plates and their strong structurally enhanced and selective adsorption performance for environmental remediation. J. Mater. Chem. 20: 8582–8590.

[53] Kumar K Y, Muralidhara H B, Arthoba Nayaka Y, Balasubramanyam J and Hanumanthappa H (2013) Hierarchically assembled mesoporous ZnO nanorods for the removal of lead and cadmium by using differential pulse anodic stripping voltammetric method. Powder Technol. 239: 208–216.

[54] Sheela T, Nayaka Y A, Viswanatha R, Basavanna S and Venkatesha T G (2012) Kinetics and thermodynamics studies on the adsorption of Zn(II), Cd(II) and Hg(II) from aqueous solution using zinc oxide nanoparticles. Powder Technol. 217: 163–170.

[55] Ma X F, Wang Y Q, Gao M J, Xu H Z and Li G A (2010) A novel strategy to prepare ZnO/PbS heterostructured functional nanocomposite utilizing the surface adsorption property of ZnO nanosheets. Catal. Today. 158: 459–463.

[56] Visa M and Duta A (2013) TiO_2/fly ash novel substrate for simultaneous removal of heavy metals and surfactants. Chem. Eng. J. 223: 860–868.

[57] Jing C, Meng X, Calvache E and Jiang G (2009) Remediation of organic and inorganic arsenic contaminated groundwater using a nanocrystalline TiO_2 based adsorbent. Environ. Pollut. 157: 2514–2519.

[58] Luo T, Cui J, Hu S, Huang Y and Jing C (2010) Arsenic removal and recovery from Copper Smelting Wastewater Using TiO_2. Environ. Sci. Technol. 44: 9094–9098.

[59] Engates K E and Shipley H J (2011) Adsorption of Pb, Cd, Cu, Zn, and Ni to titanium dioxide nanoparticles: effect of particle size, solid concentration, and exhaustion. Environ. Sci. Pollut. Res. 18: 386–395.

[60] Liang P, Shi T Q and Li J (2004) Nanometer-size titanium dioxide separation/ preconcentration and FAAS determination of trace Zn and Cd in water sample. Int. J. Environ. Anal. Chem. 84: 315–321.

[61] Zhang F Lan, J, Zhao Z, Yang Y, Tan R and Song W (2012) Removal of heavy metal ions from aqueous solution using Fe_3O_4–SiO_2-poly (1,2-diaminobenzene) core–shell sub-micron particles. J. Colloid Interface Sci. 387: 205–212.

[62] Yuan Q, Li N, Chi Y, Geng W, Yan W, Zhao Y, Li X, Dong B (2013) Effect of large pore size of multifunctional mesoporous microsphere on removal of heavy metal ions. J. Hazard. Mater. 254–255: 157–165.

[63] Sinha A and Jana N R (2012) Functional, mesoporous, superparamagnetic colloidal sorbents for efficient removal of toxic metals. Chem. Commun. 48: 9272–9274.

[64] Bagheri H, Afkhami A, Saber-Tehrani M and Khoshsafar H (2012) Preparation and characterization of magnetic nanocomposite of Schiff base/silica/magnetite as a preconcentration phase for the trace determination of heavy metal ions in water, food and biological samples using atomic absorption spectrometry. Talanta. 97: 87–95.

[65] Abollino O, Aceto M, Malandrino M, Sarzanini C and Mentasti E (2003) Adsorption of heavy metals on Na-montmorillonite. Effect of pH and organic substances. Water Res. 37: 1619-1627.

[66] Lefèvre G, Kneppers J F and Fédoroff M (2008) Sorption of uranyl ions on titanium oxide studied by ATR-IR spectroscopy. J. Colloid. Interface Sci. 327: 15-20.

[67] Lo-Irene H M C and Chen G H (2005) Fast removal and recovery of Cr(VI) using surface-modified jacobsite nanoparticles. Langmuir. 21: 11173–11179.

[68] Lee S and Anderson P R (2005) EXAFS study of Zn sorption mechanisms on hydrous ferric oxide over extended reaction time. J. Colloid. Interface Sci. 286: 82-89.

[69] Banerjee S S and Chen D-H (2007) Fast removal of copper ions by gum Arabic modified magnetic nano-adsorbent. J. Hazard. Mater. 147: 792–799.

[70] Pearson R G (1963) Hard and soft acids and bases. J. Am. Chem. Soc. 85: 3533–3539.

[71] Liang X, Xu Y, Sun G, Wang L, Sun Y and Qin X (2009) Preparation, characterization of thiol-functionalized silica and application for sorption of Pb^{2+} and Cd^{2+}. Colloids Surf. A. 349: 61–68.

[72] Ma S, Li R, Lv C, Xu W and Gou X (2011) Facile synthesis of ZnO nanorods arrays and hierarchical nanostructures for photocatalysis and gas sensor applications. J. Hazard. Mater. 192: 730–740.

[73] Kim D and Huh Y-D (2011) Morphology-dependent photocatalytic activities of hierarchical microstructures of ZnO. J. Mater. Lett. 65: 2100-2103.

[74] Li Y, Gong J and Deng Y (2010) Hierarchical structured ZnO nanorods on ZnO nanofibers and their photoresponse to UV and visible lights. Sens. Actuators, A. 158: 176–182.

[75] Xu L, Hu Yan-Ling, Pelligra C, Chen Chun-Hu, Jin L, Huang H, Sithambaram S, Aindow M, Joesten R and Suib S L (2009) ZnO with different morphologies synthesized by solvothermal methods for enhanced photocatalytic activity. Chem. Mater. 21: 2875–2885.

[76] Zhai T, Xie S, Zhao Y, Sun X, Lu X, Yu M. Xu M, Xiao F and Tong Y (2012) Controllable synthesis of hierarchical ZnO nanodisks for highly photocatalytic activity. CrystEngComm. 14: 1850–1855.

[77] Zheng J, Jiang Z-Y, Kuang Q, Xie Z-X, Huang R-B and Zheng L-S (2009) Shape-controlled fabrication of porous ZnO architectures and their photocatalytic properties. J. Solid State Chem. 182: 115–121.

[78] Singh S, Barick K C and Bahadur D (2013) Shape-controlled hierarchical ZnO architectures: Photocatalytic and antibacterial activities. CrystEngComm. 15: 4631–4639.

[79] Yıldırım Ö A, Unalan H E and Durucan C (2013) Highly efficient room temperature synthesis of silver-doped zinc oxide (ZnO:Ag) nanoparticles: structural, optical, and photocatalytic properties. J. Am. Ceram. Soc. 96: 766–773.

[80] Mohan R, Krishnamoorthy K, Kim S-J (2012) Enhanced photocatalytic activity of Cu-doped ZnO nanorods. Solid State Commun. 152: 375–380.

[81] Barka-Bouaifel F, Sieber B, Bezzi N, Josef B, Roussel P, Boussekey L, Szuneritsa S and Boukherroub R (2011) Synthesis and photocatalytic activity of iodine-doped ZnO nanoflowers. J. Mater. Chem. 21: 10982-10989.

[82] Barick K C, Singh S, Aslam M and Bahadur D (2010) Porosity and photocatalytic studies of transition metal doped ZnO nanoclusters. Micro. Meso. Mater. 134: 195–202.

[83] Qiu X, Li G, Sun X, Li L and Fu X (2008) Doping effects of Co(2+) ions on ZnO nanorods and their photocatalytic properties. Nanotechnology 19: 215703-215710.

[84] Ullah R and Dutta J (2008) Photocatalytic degradation of organic dyes with manganese-doped ZnO nanoparticles, J. Hazard. Mater. 156: 194–200.

[85] Xie M, Jing L, Zhou J, Lin J and Fu H (2010) Synthesis of nanocrystalline anatase TiO_2 by one-pot two-phase separated hydrolysis-solvothermal processes and its high activity for photocatalytic degradation of rhodamine B. J. Hazard. Mater. 176: 139–145.

[86] Pang Y L and Abdullah A Z (2013) Fe^{3+} doped TiO_2 nanotubes for combined adsorption–sonocatalytic degradation of real textile wastewater. Appl. Catalysis B: Environ. 129: 473–481.

[87] Bzdon S, Ralski J G, Maniukiewicz W, Perkowski J, Rogowski J, Szadkowska-Nicze M (2012) Radiation-

www.intechopen.com

Sarika Singh, K. C. Barick and D. Bahadur: Functional Oxide Nanomaterials and Nanocomposites for the Removal of Heavy Metals and Dyes   17

induced synthesis of Fe-doped TiO₂: Characterization and catalytic properties. Radiat. Phys. Chem. 81: 322–330.

[88] Li X, Wang L and Lu X (2010) Preparation of silver-modified TiO₂ via microwave-assisted method and its photocatalytic activity for toluene degradation. J. Hazard. Mater. 177: 639–647.

[89] Yang L, Liu P, L Xi and Li S (2012) The photocatalytic activities of neodymium and fluorine doped TiO₂ nanoparticles. Ceram. Int. 38: 4791–4796.

[90] Pozan G S and Kambur A (2013) Removal of 4-chlorophenol from wastewater: Preparation, characterization and photocatalytic activity of alkaline earth oxide doped TiO₂. Appl. Catalysis B: Environ. 129: 409–415.

[91] Bagwasi S, Tian Bu, Zhang J and Nasir M (2013) Synthesis, characterization and application of bismuth and boron Co-doped TiO₂: a visible light active photocatalyst. Chem. Eng. J. 217: 108–118.

[92] Lv C, Zhou Y, Li H, Dang M, Guo C, Ou Y and Xiao B (2011) Synthesis and characterisation of Gd³⁺ doped mesoporous TiO₂ materials. Appl. Surf. Sc. 257: 5104–5108.

[93] Radoičić M, Šaponjić Z, Janković I A, Ćirić-Marjanović G, Ahrenkiel S P and Čomor M I (2013) Improvements to the photocatalytic efficiency of polyaniline modified TiO₂ Nanoparticles. Appl. Catalysis B: Environ. 136–137: 133–139.

[94] Dong F, Guo S, Wang H, Li X and Wu Z (2011) Enhancement of the visible light photocatalytic activity of C-doped TiO₂ nanomaterials prepared by a green synthetic approach. J. Phys. Chem. C. 115: 13285–13292.

[95] Wu Z B, Dong F, Zhao W R, Wang H Q, Liu Y and Guan B H (2009) The fabrication and characterization of novel carbon doped TiO₂ nanotubes, nanowires and nanorods with high visible light photocatalytic activity. Nanotechnology. 20: 235701-235709.

[96] Liu G, Han C, Pelaez M, Zhu D, Liao S, Likodimos L, Ioannidis N, Kontos A G, Falaras P, Dunlop P S M, Byrne J A and Dionysiou D D (2012) Synthesis, characterization and photocatalytic evaluation of visible light activated C-doped TiO₂ nanoparticles. Nanotechnology 23: 294003–2940013.

[97] Yu J, Dai Gg, Xiang Q and Jaroniec M (2011) Fabrication and enhanced visible-light photocatalytic activity of carbon self-doped TiO₂ sheets with exposed {001} facets. J. Mater. Chem. 21: 1049–1057.

[98] Nolan N T, Synnott D W, Seery M K, Hinderc S J, Wassenhovend A V, Pilla S C (2012) Effect of N-doping on the photocatalytic activity of sol–gel TiO₂. J. Hazar. Mater. 211–212: 88–94.

[99] Diker H, Varlikli C, Mizrak K and Dana A (2011) Characterizations and photocatalytic activity comparisons of N-doped nc-TiO₂ depending on synthetic conditions and structural differences of amine sources. Energy. 36: 1243-1254.

[100] Cheng X, Yu X, Xing Z and Wan J (2012) Enhanced Photocatalytic activity of nitrogen doped TiO₂ anatase nano-particle under simulated sunlight irradiation. Energy Procedia. 16: 598–605.

[101] Senthilnathan J and Philip L (2010) Photocatalytic degradation of lindane under UV and visible light using N-doped TiO₂. Chem. Eng. J. 161: 83–92.

[102] Wang Y, Feng C, Zhang M, Yang J and Zhang Z (2010) Enhanced visible light photocatalytic activity of N-doped TiO₂ in relation to single-electron-trapped oxygen vacancy and doped-nitrogen. Appl. Catalysis B: Environ. 100: 84–90.

[103] Li L-H, Lu J, Wang Z-S, Yang L, Zhou X-F and Han L (2012) Fabrication of the C–N co-doped rod-like TiO₂ photocatalyst with visible-light responsive photocatalytic activity. Mater. Res. Bull. 47: 1508–1512.

[104] Zheng J, Liu Z, Liu X, Yan X, Li D and Chu W (2011) Facile hydrothermal synthesis and characteristics of B-doped TiO₂ hybrid hollow microspheres with higher photo-catalytic activity. J. Alloys Compd. 509: 3771–3776.

[105] Ohno T, Akiyoshi M, Umebayashi T, Asai K, Mitsui T and Matsumura M (2004) Preparation of S-doped TiO₂ photocatalysts and their photocatalytic activities under visible light. Appl. Catal. A: Gen. 265: 115–121.

[106] Yang X, Cao C, Erickson L, Hohn K, Maghirang R and Klabunde K (2009) Photo-catalytic degradation of rhodamine B on C, S, N, and Fe-doped TiO₂ under visible-light irradiation. App. Catal. B: Environ. 91: 657–662.

[107] Ju J, Chen X, Shi Y, Miao J and Wu D (2013) Hydrothermal preparation and photocatalytic performance of N, S-doped nanometer TiO₂ under sunshine irradiation. Powder Technol. 237: 616–622.

[108] Pei C C and Leung W Woon-Fong (2013) Enhanced photocatalytic activity of electrospun TiO₂/ZnO nanofibers with optimal anatase/rutile ratio, Catal. Commun. 37: 100–104.

[109] Lin L, Yang Y, Men L, Wang X, He D, Chai Y, Zhao B, Ghoshroy S and Tang Q (2013) A highly efficient TiO₂@ZnO n–p–n heterojunction nanorod photocatalyst. Nanoscale. 5: 588-593.

[110] Wu L, Xing J, Hou Y, Xiao F Y, Li Z and Yang H G (2013) Fabrication of regular ZnO/TiO₂ heterojunction with enhanced photocatalytic properties. Chem. Eur. J. DOI: 10.1002/chem.201300949.

[111] Zhang M, An T, Liu X, Hu X, Sheng G and Fu J (2010) Preparation of a high-activity ZnO/TiO₂ photocatalyst via homogeneous hydrolysis method with low temperature crystallization. Mater. Lett. 64: 1883–1886.

[112] Pandiselvi K and Thambidurai S (2013) Synthesis of porous chitosan–polyaniline/ZnO hybrid composite and application for removal of reactive orange 16 dye, Colloids Surf. B: Biointerfaces. 108: 229–238.

[113] Khan M M, Ansari S A, Amal M I, Lee J and Cho M H (2013) Highly visible light active Ag@TiO$_2$ nanocomposites synthesized using an electrochemically active biofilm: a novel biogenic approach. Nanoscale. 5: 4427-4435.

[114] Cheng B, Le Y and Yu J (2010) Preparation and enhanced photocatalytic activity of Ag@TiO$_2$ core–shell nanocomposite nanowires. J. Hazard. Mater. 177: 971–977.

[115] Xiao F (2012) Self-assembly preparation of gold nanoparticles-TiO$_2$ nanotube arrays binary hybrid nanocomposites for photocatalytic applications. J. Mater. Chem. 22: 7819–7830.

[116] Peralta M D L R, Pal U and Zeferino R S (2012) Photoluminescence (PL) quenching and enhanced photocatalytic activity of Au-decorated ZnO nanorods fabricated through microwave-assisted chemical synthesis. ACS Appl. Mater. Interfaces 4: 4807–4816.

[117] Wang D-H, Jia L, Wu X-L, Lu L-Q and Xu A-W (2012) One-step hydrothermal synthesis of N-doped TiO$_2$/C nanocomposites with high visible light photocatalytic activity. Nanoscale. 4: 576-584.

[118] Wang X, Blackford M, Prince K and Caruso R A (2012) Preparation of boron-doped porous titania networks containing gold nanoparticles with enhanced visible-light photocatalytic activity. ACS Appl. Mater. Interfaces. 4: 476–482.

[119] Zhang X, Zhu Y, Yang X, Wang S, Shen J, Lin B and Li C (2013) Enhanced visible light photocatalytic activity of interlayer-isolated triplex Ag@SiO$_2$@TiO$_2$ core–shell nanoparticles. Nanoscale. 5: 3359–3366.

[120] Zhang P, Shao C, Zhang Z, Zhang M, Mu J, Guo Z, Sun Y and Liua Y (2011) Core/shell nanofibers of TiO$_2$@carbon embedded by Ag nanoparticles with enhanced visible photocatalytic activity. J. Mater. Chem. 21: 17746–17753.

[121] Zhang P, Shao C, Li X, Zhang M, Zhang X, Sun Y and Liu Y (2012) In situ assembly of well-dispersed Au nanoparticles on TiO$_2$/ZnO nanofibers: a three-way synergistic heterostructure with enhanced photocatalytic activity. J. Hazard. Mater. 237–238: 331–338.

[122] Wang D, Duan Y, Luo Q, Li X, An J, Bao L and Shi L (2012) Novel preparation method for a new visible light photocatalyst: mesoporous TiO$_2$ supported Ag/AgBr. J. Mater. Chem. 22: 4847–4854.

[123] Tang Y, Jiang Z, Deng J, Gong D, Lai Y, Tay H T, Joo I T K, Lau T H, Dong Z and Chen Z (2012) Synthesis of nanostructured silver/silver halides on titanate surfaces and their visible-light photocatalytic performance. ACS Appl. Mater. Interfaces. 4: 438–446.

[124] Liu J, Zuoa S, Yua L, Yua Y, Lia B and Chen P (2013) Visible light photodegradation of methylene blue by AgBr–TiO$_2$/SiO$_2$@Fe$_3$O$_4$ magnetic photocatalysts, Particuology,http://dx.doi.org/10.1016/j.partic.2013.01.006.

[125] Yang Z-P, Gong X-Y and Zhang C-J (2010) Recyclable Fe$_3$O$_4$/hydroxyapatite composite nanoparticles for photocatalytic applications. Chem. Eng. J. 165: 117–121.

[126] Xia J, Wang A, Liu X, Su Z (2011) Preparation and characterization of bifunctional, Fe$_3$O$_4$/ZnO nanocomposites and their use as photocatalysts. Appl. Surf. Sci. 257: 9724–9732.

[127] Ye M, Zhang Q, Hu Y, Ge J, Lu Z, Chen L Z and Yin Y (2010) Magnetically recoverable core–Shell nanocomposites with enhanced photocatalytic activity. Chem. Eur. J. 16: 6243–625.

[128] Nabid M R, Sedghi R, Gholami S, Oskooie H A and Heravi M M (2013) Preparation of new magnetic nanocatalysts based on TiO$_2$ and ZnO and their application in improved photocatalytic degradation of dye pollutant under visible light. Photochem. Photobiol. 89: 24–32.

[129] Bajaj R, Sharma M and Bahadur D (2013) Visible light-driven novel nanocomposite (BiVO$_4$/CuCr$_2$O$_4$) for efficient degradation of organic dye. Dalton Trans. 42: 6736–6744.

[130] Lin Y, Zhang F, Pan D, Li H and Lu Y (2012) Sunlight-driven photodegradation of organic pollutants catalyzed by TiO$_2$/(ZnS)$_x$(CuInS$_2$)$_{1-x}$ nanocomposites. J. Mater. Chem. 22: 8759–8763.

[131] Li G, Zhang D, Yu J C and Leung M K H (2010) An efficient bismuth tungstate visible-light-driven photocatalyst for breaking down nitric oxide. Environ. Sci. Technol. 44: 4276–4281.

[132] Yao W, Zhang B, Huang C, Ma C, Song X and Xu Q (2012) Synthesis and characterization of high efficiency and stable Ag$_3$PO$_4$/TiO$_2$ visible light photocatalyst for the degradation of methylene blue and rhodamine B solutions. J. Mater. Chem. 22: 4050–4055.

[133] Dong H, Chen G, Sun J, Li C, Yu Y and Chen D (2013) A novel high-efficiency visible-light sensitive Ag$_2$CO$_3$ photocatalyst with universal photodegradation performances: simple synthesis, reaction mechanism and first-principles study. Appl. Catalysis B: Environ. 134–135: 46–54.

[134] Jiang B, Zhang P, Zhang Y, Wu L, Li H, Zhang D and Li G (2012) Self-assembled 3D architectures of Bi$_2$TiO$_4$F$_2$ as a new durable visible-light photocatalyst. Nanoscale. 4: 455–460.

[135] Zheng Y H, Chen C Q, Zhan Y Y, Lin X Y, Zheng Q, Wei K M, Zhu J F and Zhu Y J (2007) Luminescence and photocatalytic activity of ZnO nanocrystals: correlation between structure and property. Inorg. Chem. 46: 6675–6682.

www.intechopen.com

Sarika Singh, K. C. Barick and D. Bahadur: Functional Oxide Nanomaterials and Nanocomposites for the Removal of Heavy Metals and Dyes   19